Received: 8 March 2024 | Accepted: 4 July 2024

DOI: 10.1111/2041-210X.14402

Methods in Ecology and Evolution

RESEARCH ARTICLE

Physically based modelling of spectral transmittance through forest canopies

Aarne Hovi[1] | Růžena Janoutová[2] | Zbyněk Malenovský[3] | Daniel Schraik[4] | Jean-Philippe Gastellu-Etchegorry[5] | Nicolas Lauret[5] | Jan Novotný[2] | Miina Rautiainen[1]

[1]School of Engineering, Aalto University, Espoo, Finland

[2]Global Change Research Institute of the Czech Academy of Sciences, Brno, Czech Republic

[3]Remote Sensing Research Group, Department of Geography, University of Bonn, Bonn, Germany

[4]Natural Resources Institute Finland, Helsinki, Finland

[5]CESBIO, UT3-Paul Sabatier, CNES/CNRS/INRAE/IRD/Université de Toulouse, Toulouse, France

Correspondence
Aarne Hovi
Email: aarne.hovi@aalto.fi

Růžena Janoutová
Email: janoutova.r@czechglobe.cz

Funding information
European Research Council, Grant/Award Number: 771049; Ministerstvo Školství, Mládeže a Tělovýchovy, Grant/Award Number: LTAUSA18154

Handling Editor: Abebe Ali

Abstract

1. Physically based models simulating the spectral transmittance of solar radiation through forest canopies are useful tools for examining the connections between the shortwave radiation environment and the productivity and biodiversity of the forest floor. We report a comprehensive evaluation of two approaches simulating forest canopy spectral transmittance.
2. The approaches were (i) three-dimensional radiative transfer modelling in canopies composed of individual trees filled with turbid media and (ii) photon recollision probability theory (*p*-theory), and were implemented using DART-FT and PARAS models, respectively. The simulations were evaluated against mean and standard deviation of canopy transmittance spectra measured under clear-sky conditions in forest plots across central and Northern Europe.
3. In general, both models agreed well with the in situ measurements. They performed equally in conifer forests, while PARAS had a slightly lower accuracy than DART-FT in broadleaved forests.
4. We conclude that both approaches produce realistic simulations of canopy spectral transmittance at the spatial scale tested in this study, and that *p*-theory constitutes a computationally efficient and easy-to-parameterize alternative to three-dimensional radiative transfer.

KEYWORDS
DART, forest, PARAS, photon recollision probability, radiative transfer modelling, remote sensing, shortwave radiation regime, spectral transmittance

1 | INTRODUCTION

Solar radiation under forest canopies influences understorey growth conditions and photosynthesis. It also affects the microclimate, which in turn impacts species richness and functional diversity (De Pauw et al., 2021) as well as forest hydrological processes (Ellis et al., 2011; Musselman et al., 2015). In addition to the quantity of solar radiation, its spectral distribution

Aarne Hovi and Růžena Janoutová—joint first authorship.

is also modulated by plant canopies (Hertel et al., 2011; Hovi & Rautiainen, 2020; Smith, 1982). The spectral characteristics of transmitted solar radiation act as signals that plants use to detect and respond to competition (Ballaré & Austin, 2019), and that potentially also affect their phenology (Brelsford et al., 2019). Moreover, the interpretation of remote sensing data requires accurate knowledge of the spectral irradiance at the point seen by the remote sensing instrument (Damm et al., 2015). Hence, understanding the spectral transmittance characteristics of forest canopies is important for applications ranging from forest ecology to optical remote sensing.

In situ measurements with spectrometers (Hartikainen et al., 2020; Hertel et al., 2011; Hovi & Rautiainen, 2020) provide information on how forest canopy spectral transmittance depends on factors such as the canopy structure and tree species composition. Simulations of spectral transmittance with physical models of radiation transfer (Kükenbrink et al., 2021), are useful in understanding the physical mechanisms and extending the interpretations beyond pointwise measurements. Although canopy spectral transmittance is routinely outputted by several radiation transfer models, the RAdiation transfer Model Intercomparison exercise (RAMI) (Widlowski et al., 2011, 2015) showed large discrepancies in canopy transmittance simulated by different models. Comparison of models with empirical measurements can help to identify which parameterizations produce results closest to reality. Studies that have compared simulated canopy transmittance to empirical observations are usually limited to broadband quantities in the visible or photosynthetically active wavelength region (e.g. Majasalmi et al., 2014; Ni et al., 1997). For spectral properties of transmitted radiation, we found only a single study that compared simulated single tree transmittance with empirical observations (Kükenbrink et al., 2019). Thus, although spectral properties of solar radiation transmitted by forest canopies have been measured and simulated, direct comprehensive comparisons of measurements with models have rarely been performed.

In this study, we (i) assess the performance of two approaches for modelling the spectral properties of solar radiation transmitted through forest canopies by comparing them to a unique set of in situ measurements conducted in temperate and boreal forests, and (ii) evaluate their differences and limitations from a practical point of view. The approaches are (i) radiative transfer modelling in scenes composed of turbid individual tree crowns ('turbid-medium crown'), and (ii) photon recollision probability theory ('*p*-theory'). Models employing these approaches can be parameterized with typical in situ forest inventory and canopy gap fraction measurements, or using existing forest databases. The turbid-medium crown approach requires information on individual tree positions and crown dimensions. Although it makes simplifying assumptions about the within-crown spatial distribution of foliage, it represents a detailed parameterization in many land surface models (Ni-Meister et al., 2010). The *p*-theory approach is a computationally efficient alternative in which the canopy structure can be described solely based on canopy gap fractions.

2 | MATERIALS AND METHODS

2.1 | Definition of canopy spectral transmittance

Given that the spectral irradiance at the top-of-canopy (bottom-of-atmosphere) is known from measurements or models, spectral irradiance at a given point below the forest canopy can be predicted from the canopy spectral transmittance. We define spectral transmittance here as the spectral irradiance at a horizontal plane below the canopy at 1.5 m height, divided by the corresponding irradiance above the canopy. It includes radiation transmitted through the canopy with and without scattering (i.e. diffuse and direct transmittance), and also the radiation reflected by the forest floor, which is then scattered downwards by the canopy.

2.2 | Measurements of canopy spectral transmittance

Canopy spectral transmittance was measured in 21 plots located in four study sites in Finland, Estonia and the Czech Republic. The sites at Hyytiälä (HY; 61°51′ N, 24°18′ E), Järvselja (JS; 58°17′ N, 27°19′ E), Bílý Kříž (BK; 49°30′ N, 18°32′ E) and Lanžhot (LZ; 48°41′ N, 16°57′ E) represent boreal conifer-dominated, hemiboreal mixed, temperate coniferous mountain and temperate broadleaved forests, respectively (Table S1). The measurements were conducted under clear-sky conditions in the summers of 2019 and 2020 (June to September), between 9:10 AM and 5:26 PM local time, when the solar elevation varied between 29° and 50°. The measurements in each plot took 13 min–25 min, comprising a total of 49 canopy spectral transmittance measurements at 1.5 m height, in a grid of 7 × 7 measurements with 5 m distance between measurements (i.e. covering an area of 30 m × 30 m) (Figure S1). We used ASD FieldSpec3 and FieldSpec4 spectrometers coupled with ASD diffuser-type cosine receptors (model A124505). One of the spectrometers was located in an open area and was taking measurements every 15 s, while the other spectrometer was operated in the forest. The spectrometers were radiometrically intercalibrated at the beginning and end of each measurement session (every session comprising measurements of one or several plots). The maximum duration of a session was 3 h 20 min. The canopy transmittance was calculated as the ratio of the raw spectrometer reading taken in the forest to that interpolated from the two temporally closest reference measurements, that is, those taken immediately before and after the canopy transmittance measurement. The data processing details are described in Hovi and Rautiainen (2020).

The spectrometers delivered data at 350–2500 nm, but we removed spectral regions that were noisy due to radiation absorption by atmospheric water vapour (1350–1450 nm and 1800–1980 nm) or by the technical limitations of the cosine receptors (2200–2500 nm). We use the plot-level averages and standard deviations of the transmittance spectra in our analyses.

2.3 | Modelling of canopy spectral transmittance

We tested turbid-medium crown and *p*-theory approaches for modelling the canopy spectral transmittance. Both approaches require information on the canopy structure (i.e. structural parameters) and on the spectral properties of the canopy elements and the forest floor (i.e. spectral parameters). The main difference lies in how the canopy structure is parameterized. In the turbid-medium crown approach, individual tree crowns are represented as geometric shapes that are filled with turbid media representing foliage and woody elements. In the *p*-theory approach, the canopy structure is parameterized based on canopy gap fractions. Hence, it requires only few input parameters and is, due to its relative simplicity, computationally highly efficient.

We used functions in the Discrete Anisotropic Radiative Transfer (DART) model version 5100 v1344 to model the turbid-medium crowns and its flux tracking mode to simulate the forest canopy spectral transmittance. The DART modelling (Gastellu-Etchegorry et al., 2015, 2016; Malenovský et al., 2021) was used as a reference approach, as it has been validated in the RAMI exercise and agreed well with other 3D radiative transfer models (Widlowski et al., 2013, 2015). For the *p*-theory approach, we utilized the PARAS model (Rautiainen & Stenberg, 2005), employing its version reported by Hovi et al. (2022). For simplicity, we use the model names, DART-FT and PARAS, in reporting our results. However, we note that the results should be interpreted as a comparison between modelling approaches rather than between two specific models, because the DART model can also be parameterized in other ways than using turbid-medium crowns.

We simulated canopy spectral transmittance with both models at the central wavelengths of the Sentinel-2A MSI satellite instrument's bands at 493, 560, 665, 704, 741, 783, 865, 1614 and 2202 nm. For each plot, we conducted the simulations at the solar position matching the midpoint of the canopy spectral transmittance measurements. The wavelength-dependent diffuse and direct fractions of solar irradiance at the top-of-canopy were used to characterize the radiation conditions in both models, and were calculated using the default discrete-ordinates method in the libRadtran radiative transfer library version 2.0.4 (Emde et al., 2016; Mayer & Kylling, 2005). The atmospheric parameters (aerosol optical depth and water vapour) were obtained from the Copernicus Atmospheric Monitoring Service (CAMS) global reanalysis product EAC4 (Inness et al., 2019), downloaded from the Copernicus web page (CAMS, 2023).

2.4 | Model input data

2.4.1 | Canopy structural inputs

Forest inventory measurements were conducted in each plot within a 25 m × 25 m area (Figure S1). Species and diameter at breast height (DBH, 1.3 m) were recorded for trees that exceeded a predefined diameter limit: 8 cm for mature forest (height >16 m) and 5 cm elsewhere. Positions of the trees were determined by recording the azimuth and distance of the tree in relation to the plot centre.

We used terrestrial laser scanning (TLS) data to obtain the height and crown dimensions of trees. TLS data were acquired on every other measurement point on the same grid of the canopy spectral transmittance measurements, resulting in 16 measurements covering an area of 30 m × 30 m (Figure S1). The individual scans were co-registered to form a single point cloud per plot. The TLS data acquisition and preprocessing are described in Schraik et al. (2023). We used a decimated point cloud with an average point spacing of 2 cm, enabling fast and easy processing. The field-measured tree positions were linked with TLS data, allowing us to manually measure treetop positions and crown dimensions (tree height, length of tree crown and maximum crown diameter in east–west and north–south directions) from TLS data. The manual measurement could not be performed for trees badly occluded by their neighbours, mainly small trees in suppressed canopy layers. Their crown dimensions were predicted using plot- and species-specific regression models, where DBH was the predictor variable. Finally, we used the TLS data to detect and measure trees that were not present in the forest inventory data, mainly due to imprecisions in field delineation of the 25 m × 25 m area. We predicted DBH for these trees using regression models where crown diameter was the predictor. As a result, we had a complete map of trees within the 25 m × 25 m forest inventory area.

We used hemispherical photographs for calculating the effective and clumping-corrected plant area index (PAI_{eff} and PAI) and canopy interception of solar radiation required for the model simulations. Hemispherical photographs were acquired under diffuse illumination conditions at the same 16 positions as the TLS acquisitions (Figure S1). We used a Nikon D5000 camera with a geometrically calibrated Sigma EX 4.5 mm f/2.8 DC HSM Circular Fisheye lens. The camera was placed at 1.5 m height and accurately levelled to point upwards. The blue band of the photographs was binarized using a thresholding algorithm that maximizes the brightness difference between canopy and sky pixels (Nobis & Hunziker, 2005). The photography and image processing are detailed in Hovi et al. (2022).

2.4.2 | Spectral inputs

The spectral input used in the models (i.e. spectra of foliage, woody elements and forest floor) were adopted from the forest reflectance modelling conducted by Hovi et al. (2022), who also describe spectral measurements and processing details. Below, we provide an overview of the utilized spectra.

Leaf and needle directional-hemispherical reflectance and transmittance spectra were measured in our study sites using integrating spheres coupled with spectrometers. Representative average foliage spectra were calculated per tree species of each study site by giving appropriate weights to the top-of-canopy and bottom-of-canopy foliage, and additionally to the current-year and older needle age cohorts in conifers. Some minority species were not measured: For these species, we used the average of all conifers or the average

of all broadleaved species in the site or in the geographically closest site. We used a shoot as the basic foliage element for conifers in both PARAS and DART-FT models. We calculated shoot albedo (ω_{sh}, reflectance + transmittance) from needle albedo (ω_n) as $\omega_{sh} = (1-p) \times \omega_n / (1 - p\omega_n)$ (Rautiainen et al., 2012), where p is photon recollision probability calculated as $p = 1 - \beta_{sh}$, and β_{sh} is the shoot clumping coefficient (assumed to be 0.6 for all conifers). Shoot transmittance (T_{sh}) was calculated from needle transmittance (T_n) with an empirical equation $T_{sh} = (-0.553/\beta_{sh} + 1.553) \times T_n$ (Rautiainen et al., 2018), and shoot reflectance (R_{sh}) was obtained as $R_{sh} = \omega_{sh} - T_{sh}$. For broadleaf species, we used the leaf reflectance and transmittance without any modifications.

Woody element spectra were obtained from two sources. Stem bark hemispherical-directional reflectance factor (HDRF) spectra, measured with a spectral camera in Finland and Estonia (Juola et al., 2022a, 2022b), were used for wavelengths up to 1000 nm. All major tree genera present in our study plots were included in these measurements. Ideally, the models would require as input the hemispherically integrated reflectance. However, bark spectral measurements are rare, and these measurements were the best available for our study sites and species. For wavelengths above 1000 nm, we used data from other published sources: pine, spruce and birch stem bark spectra were taken from Lang et al. (2002), while the aspen stem bark spectrum from Spencer and Rock (1999) was used for all other broadleaved species. Spectral continuity was ensured by multiplying these spectra with a scaling factor, so that the reflectance at 1000 nm matched with the measurements of Juola et al. (2022a, 2022b) at the same wavelength. Stem bark reflectance spectra were used as proxies of reflectance spectra of all woody elements (stems, branches and twigs) in both PARAS and DART-FT models. Transmittance of woody elements was assumed to be zero.

Forest floor hemispherical-conical reflectance factors were obtained as an average of 15 in situ measurements conducted along an 11-m long transect at the centre of each forest plot (Figure S1). The measurements were conducted in diffuse illumination conditions, using a field spectrometer with a bare fibre-optic cable (25° field-of-view) as the detector. Plot-level average reflectance factors were used to represent forest floor spectral properties in the PARAS and DART-FT models. To harmonize the data and to ensure that the simulation results were not affected by noise present in the input spectra, all spectra were interpolated into a resolution of 1 nm and smoothed with a Savitzky–Golay filter (Savitzky & Golay, 1964). The 1-nm bands that correspond to the central wavelengths of the selected Sentinel-2 MSI bands (Section 2.3) were used in the simulations.

2.5 | Model parameterization and simulations

2.5.1 | Turbid-medium crown approach (DART-FT)

We generated 3D models of the forest plots (Figure S2), based on measurements of individual trees representing the 25 m × 25 m area of forest inventory. We used the option 'exact locations + exact dimensions' in DART-FT, as explained below.

Tree stems were modelled as solid objects composed of parallelepipeds. Tree height and DBH were taken from the forest inventory and TLS measurements, and stem reflectance from the in situ spectral measurements. The forest floor was modelled as a solid, flat surface, with its reflectance measured in situ. Both stems and forest floor surfaces were assumed to be Lambertian. Tree crowns were created from two half-ellipsoids representing the upper and lower crown parts (Figure S3), respectively, with crown positions and dimensions retrieved from the TLS measurements (Section 2.4.1). The tree canopy was composed of a regular grid of 0.5 m × 0.5 m × 0.5 m voxels that were filled with a turbid medium, if belonging to a tree crown. The turbid medium contained two types of scattering elements: woody elements (branches and twigs) and foliage (leaves for broadleaf trees and shoots for conifers). Each element type in a voxel was characterized by its orientation, area volume density [$m^2\,m^{-3}$] and optical properties.

The azimuthal orientation of all elements was assumed to be random, whereas zenith angle distributions of the foliage were modelled with species-specific beta distributions parameterized by measurements of leaf and shoot angles reported in the literature (Table S2). We assumed that the woody elements had the same zenith angle distributions as the foliage. The plant (foliage + woody elements) area volume density (PAVD) was assumed to be constant across all canopy voxels within a plot. To obtain PAVD, we designed an inversion routine that was operated outside of DART-FT and took as input a 3D scene representation similar to that used in DART-FT. All canopy elements were assumed to be optically black (non-scattering), and ray tracing was applied to estimate canopy gap fractions and to simulate hemispherical photos. We iteratively searched for an optimal PAI so that the PAI_{eff} values (calculated based on canopy gap fractions) matched between the simulated and real hemispherical photos. PAI was used in DART-FT to calculate PAVD, which was further divided into foliage and woody area volume densities according to species-specific woody to total plant area fractions. We applied woody to total plant area fractions from Hovi et al. (2022): 0.32 for pine, 0.30 for spruce and 0.12 for broadleaved species. If a voxel belonged to two trees of different species (overlapping crowns), 50% of the PAVD was assigned to one species and 50% to the other. For the optical properties of the canopy elements, we used the foliage and woody element reflectance and transmittance spectra (Section 2.4.2). All elements were assumed to be Lambertian surfaces.

We used cyclic boundary conditions in our DART-FT simulations, that is, whenever a photon escaped the scene from its side, it re-entered the scene from the opposite side. The DART-FT output was a 3D radiative budget file per simulated wavelength, which stores the radiation fluxes entering and leaving each voxel. From the 3D radiative budget values, we calculated spatially explicit estimates of canopy spectral transmittance. For each voxel at 1.5 m height, the transmittance was calculated as the downward flux entering the voxel from above divided by the downward flux at the

corresponding voxel at top-of-canopy. The average and standard deviation of spectral transmittance were then obtained from the spatially explicit values.

2.5.2 | Photon recollision probability theory (PARAS)

The calculation of canopy spectral transmittance (T) in the PARAS model was given by Hovi et al. (2022) as

$$T = \frac{T_{BS}}{1 - R_G R_S}, \quad (1)$$

where T_{BS} is the canopy transmittance when the forest floor is optically black, R_G is the forest floor reflectance, and R_S is the reflectance of the canopy for radiation that is entering the canopy from below (i.e. reflected by the forest floor). The denominator $(1 - R_G R_S)$ models multiple scattering between the forest floor and the canopy. The wavelength-dependence is ignored in the equations for simplicity. The terms R_S and T_{BS} are calculated as

$$T_{BS} = (1 - i_0) + i_0 \omega_C (1 - Q), \text{and} \quad (2)$$

$$R_S = i_D \omega_C Q, \quad (3)$$

where i_0 is the canopy interception of incoming radiation (comprising direct and diffuse components), i_D is the canopy interception of diffuse radiation, Q is the reflectance to scattering ratio of the canopy and ω_C is the canopy scattering coefficient, calculated as

$$\omega_C = \frac{(1 - p)\omega_E}{1 - p\omega_E}, \quad (4)$$

where p is photon recollision probability and ω_E is the plant element albedo. The canopy elements are assumed to be angularly isotropic scatterers in PARAS. We calculated Q according to Mõttus and Stenberg (2008) as

$$Q = \frac{1}{2} + \frac{q}{2} \frac{1 - p\omega_E}{1 - pq\omega_E}, \quad (5)$$

where q is a scattering asymmetry parameter. The formula for q was defined in Stenberg et al. (2013) as $q = 1 - \exp(-0.1684 \times \text{LAI})$. It was derived using Monte Carlo ray tracing in six forest stands under diffuse illumination conditions. By comparing the predictions obtained from Equation (5) against Q values calculated from DART-FT's output, we found that the formula for q resulted in biased Q values in our dataset. Consequently, we recalibrated the equation for q using DART-FT simulations as $q = 1 - \exp(-0.3671 \times \text{PAI}_{\text{eff}})$ ($r^2 = 0.85$, root-mean-square-error (RMSE) = 0.065). Note that this was the only intercalibration of the models that was performed.

The structural parameters for PARAS are canopy interception of incoming radiation (i_0), canopy interception of diffuse radiation (i_D) and the photon recollision probability (p). The i_0 was calculated as the weighted sum of canopy interception of direct solar radiation (i_S) and i_D, where the diffuse and direct fractions of incoming solar irradiance are used as weights. The values of i_D and i_S in a given solar geometry were calculated from the binary hemispherical photographs. The i_D was obtained by integrating the canopy interception over the hemisphere. For calculation of i_S, we used pixels corresponding to the actual sun-zenith angle ±2.5°. We further divided each image into 5° azimuth segments. The value of i_S was then calculated for each segment in each binary image, resulting in a total of 1152 segments per plot (16 images − 72 azimuth segments per image). We calculated 1152 canopy transmittance spectra for each study plot, corresponding to the i_S values. This allowed us to estimate both the mean and standard deviation of canopy transmittance. The other parameters (i_D, p and ω_E), were assumed to be spatially invariant within a plot. We calculated p, using a formula from Stenberg (2007) as $p = 1 - i_D/\text{PAI}$. PAI was calculated from the hemispherical photos and corrected for clumping at levels larger than a shoot using the method of Lang and Xiang (1986). We did not use the same PAI as for the DART-FT model, because we wanted to test the use of the PARAS model without detailed 3D structural information from TLS data. The plant element albedo (ω_E) was calculated as a weighted average of species-specific foliage and woody element albedos (Section 2.4.2). The forest floor was assumed to be a Lambertian surface with the reflectance measured in situ.

3 | RESULTS

3.1 | Comparison of simulated and measured canopy transmittance spectra

Visual evaluation of the simulated transmittance spectra indicated that the models were able to reproduce the general spectral transmittance characteristics of the 21 forest stands represented by our study plots (Figure 1). These include (i) large between-stand variation in the transmittance at all wavelengths, mainly due to the varying PAI and canopy gap fractions (Figure S4), and (ii) the increase in the mean transmittance from red to near-infrared (NIR) wavelengths being greater for broadleaved than for coniferous forests (Figure 1).

Quantitative evaluation of the models revealed that the model errors were the smallest in the visible (blue, green and red), red-edge 1 (RE1) and shortwave-infrared 2 (SWIR2) bands (Figure 2; Table 1). The RMSE of the PARAS and DART-FT models in these bands, when compared to measurements, varied between 0.042 and 0.052 (38%–49%) for broadleaved and between 0.031 and 0.038 (21%–26%) for conifer forests (Table 1). The mean difference between simulated and measured transmittance was 0.025–0.035 for broadleaved and 0.003–0.021 for conifers (Table 1), indicating that the transmittance was slightly overestimated by both models. The difference was mainly caused by a couple of plots where both models clearly overestimated the transmittance (e.g. plot no. 5, 6, 15 and 20, Figure 1). The transmittance values simulated by the two models in the visible, RE1 and SWIR2 bands were very strongly correlated ($r^2 = 0.99$).

Slightly larger model errors (in absolute terms) were observed in the RE2, RE3 and NIR bands (Figure 2; Table 1). In these bands,

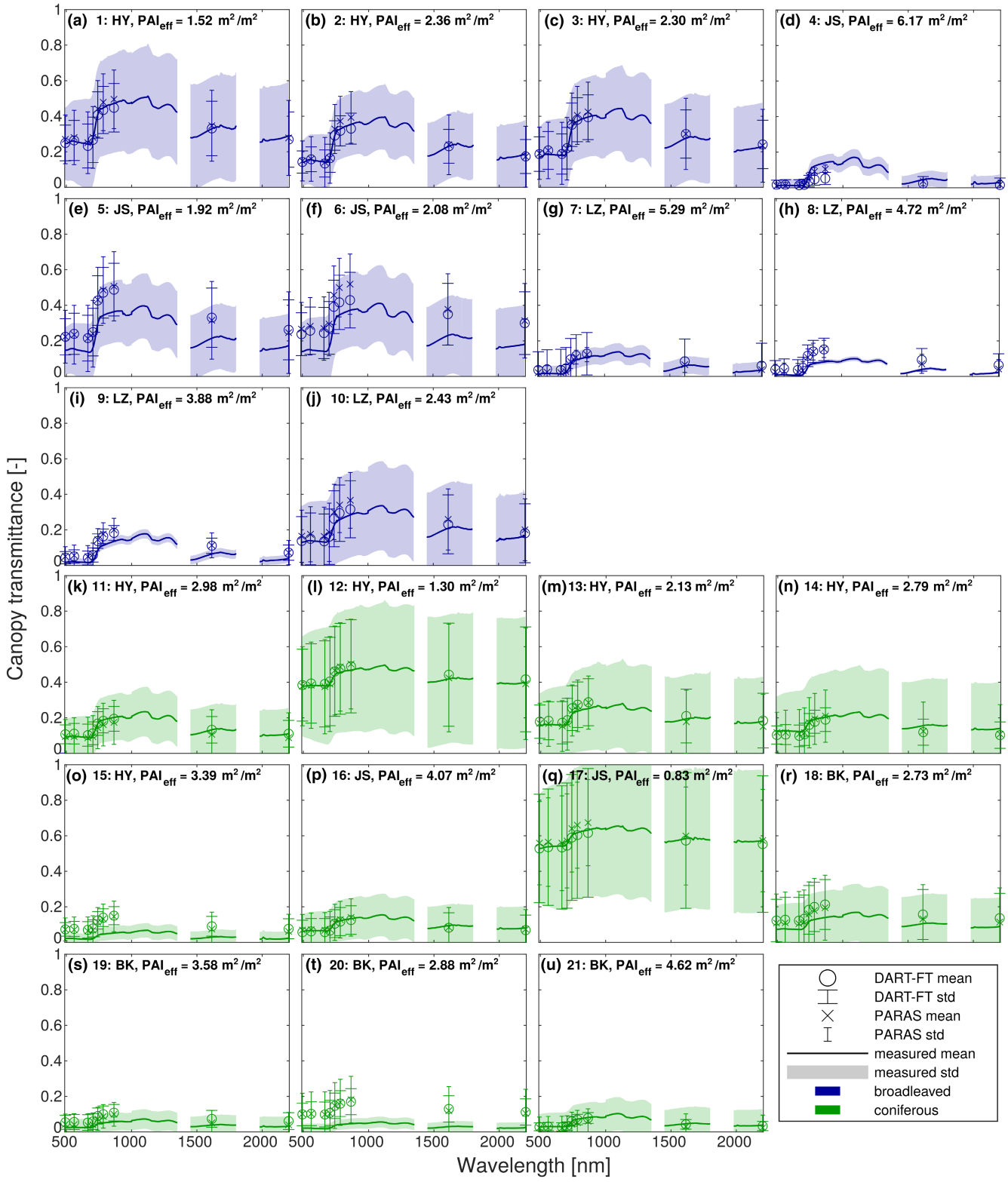

FIGURE 1 Mean and standard deviation (std) of canopy transmittance spectra in 21 forest plots simulated with DART-FT and PARAS models in comparison with in situ measurements. The plots are ordered by (i) the dominant tree type (broadleaved or coniferous, represented by the blue and green colours), and (ii) by the site from north to south (HY = Hyytiälä, JS = Järvselja, BK = Bílý Kříž and LZ = Lanžhot). Effective plant area index (PAI_{eff}) is given for each plot.

DART-FT and PARAS models performed similarly in conifer forests, where the mean difference between the simulated and measured transmittance was 0.031–0.032 for DART-FT and 0.028–0.036 for PARAS, and the respective RMSE values were 0.051–0.057 (28%) and 0.047–0.058 (26%–28%) (Table 1). In broadleaved forests, DART-FT outperformed PARAS: the mean difference was

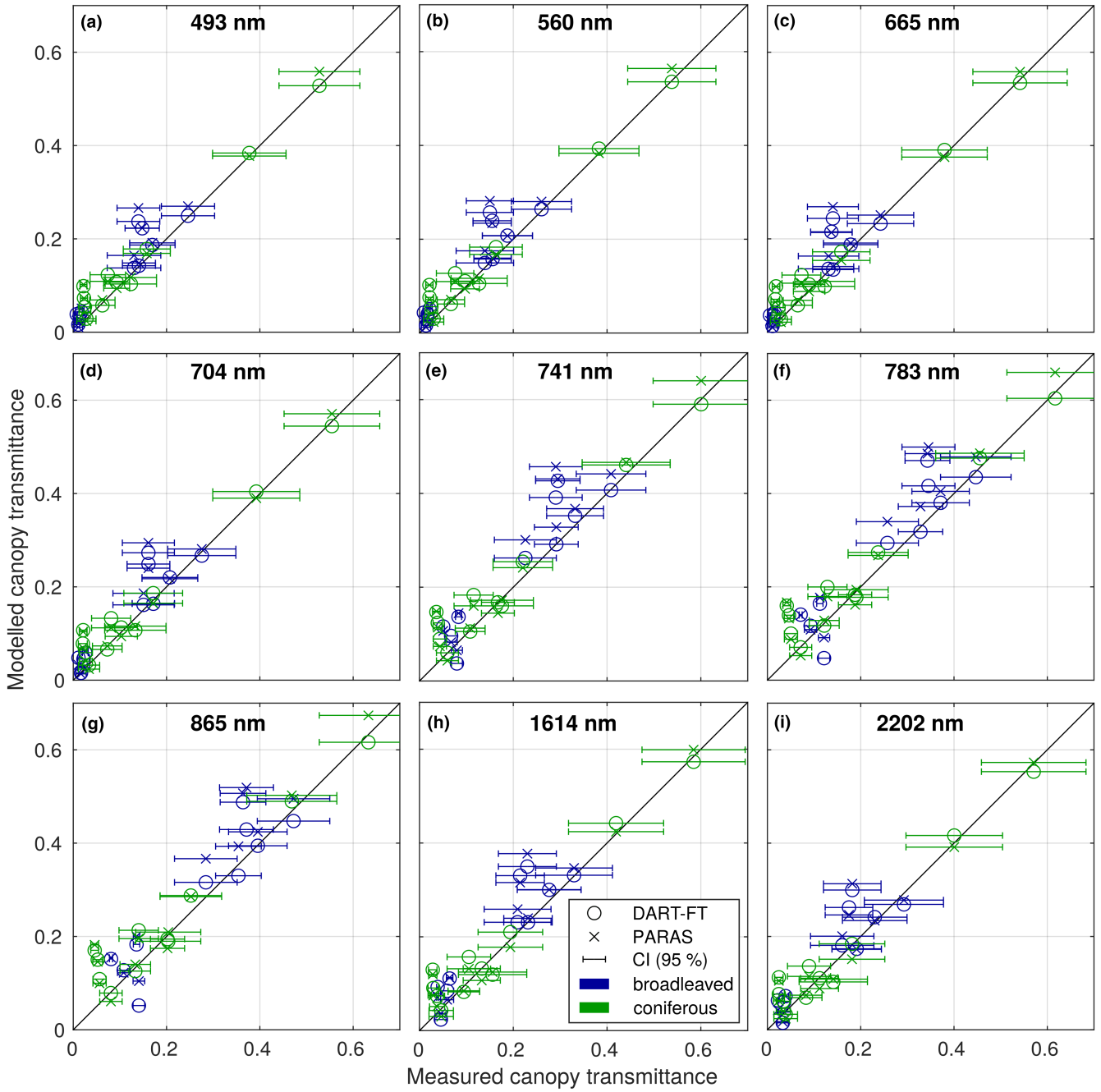

FIGURE 2 Comparison of measured canopy transmittance to simulations with DART-FT and PARAS models at nine spectral bands. Each point represents the mean transmittance of a forest plot, with broadleaved-dominated plots in blue and coniferous-dominated in green colour. The symbols indicate the models (PARAS or DART-FT) and the error bars mark the 95% confidence intervals (CI) of the in situ measured canopy transmittance, calculated as CI = mean ± 1.96 × (standard error of the mean).

0.021–0.039 for DART-FT and 0.058–0.061 for PARAS, and the respective RMSE values were 0.060–0.062 (22%–29%) and 0.079–0.081 (29%–37%) (Table 1). The correlation between the simulated transmittance by the two models in the RE2, RE3 and NIR bands was slightly weaker than in the other bands; yet the coefficient of determination was high ($r^2 \geq 0.97$) and the differences between models in the broadleaved forests were prevailingly systematic (Figure 2).

In addition to spectral transmittance at individual bands, we also investigated the red-to-NIR transmittance ratio (often referred to as red-to-far-red ratio in ecological studies) as an indicator of spectral quality of radiation under the forest canopies. The red-to-NIR ratio depended on canopy density and also differed between broadleaved and conifer canopies of the same density (same PAI). These dependencies were reproduced by the models (Figure 3).

We also evaluated the capability of the models in reproducing spatial variation (within-stand standard deviation) of canopy transmittance. The standard deviation of the measured transmittance was the largest for sparse stands (small PAI), which was reproduced by both models (Figures 1 and 4).

TABLE 1 Statistics quantifying the differences between simulated and measured canopy spectral transmittance (DART-FT-measured, PARAS-measured), and between simulations by the two models (PARAS-DART-FT) in broadleaved and conifer forests.

	r^2			Mean difference			RMSE			Relative RMSE (%)		
Wavelength	DART-FT-measured	PARAS-measured	PARAS-DART-FT	DART-FT-measured	PARAS-measured	PARAS-DART-FT	DART-FT-measured	PARAS-measured	PARAS-DART-FT	DART-FT-measured	PARAS-measured	PARAS-DART-FT
Broadleaved												
493 nm (blue)	0.88	0.87	0.99	0.029	0.035	0.006	0.042	0.050	0.016	41	49	12
560 nm (green)	0.87	0.86	0.99	0.032	0.035	0.003	0.047	0.052	0.015	42	47	10
665 nm (red)	0.83	0.84	0.99	0.026	0.032	0.006	0.044	0.050	0.015	43	49	12
704 nm (RE1)	0.84	0.84	0.99	0.030	0.032	0.002	0.049	0.052	0.014	40	43	9
741 nm (RE2)	0.88	0.89	0.98	0.039	0.060	0.021	0.062	0.079	0.031	29	37	12
783 nm (RE3)	0.86	0.90	0.98	0.029	0.061	0.031	0.060	0.081	0.041	24	32	15
865 nm (NIR)	0.85	0.89	0.97	0.021	0.058	0.037	0.060	0.079	0.046	22	29	16
1614 nm (SWIR1)	0.85	0.87	0.98	0.039	0.043	0.004	0.059	0.062	0.018	35	37	8
2202 nm (SWIR2)	0.81	0.82	0.99	0.028	0.025	−0.002	0.052	0.051	0.014	38	38	8
Conifers												
493 nm (blue)	0.97	0.97	0.99	0.020	0.020	0.000	0.034	0.033	0.013	25	24	8
560 nm (green)	0.97	0.97	0.99	0.021	0.018	−0.003	0.036	0.032	0.014	26	23	9
665 nm (red)	0.97	0.97	0.99	0.019	0.015	−0.004	0.035	0.031	0.014	26	22	9
704 nm (RE1)	0.96	0.97	0.99	0.020	0.013	−0.007	0.038	0.032	0.016	26	22	10
741 nm (RE2)	0.95	0.95	0.99	0.031	0.028	−0.002	0.051	0.047	0.020	28	26	10
783 nm (RE3)	0.94	0.94	0.99	0.032	0.033	0.001	0.054	0.054	0.021	28	28	9
865 nm (NIR)	0.94	0.94	0.99	0.032	0.036	0.004	0.057	0.058	0.022	28	28	9
1614 nm (SWIR1)	0.95	0.96	0.99	0.021	0.009	−0.012	0.043	0.035	0.020	26	21	11
2202 nm (SWIR2)	0.96	0.96	0.99	0.014	0.003	−0.011	0.038	0.032	0.019	24	21	11

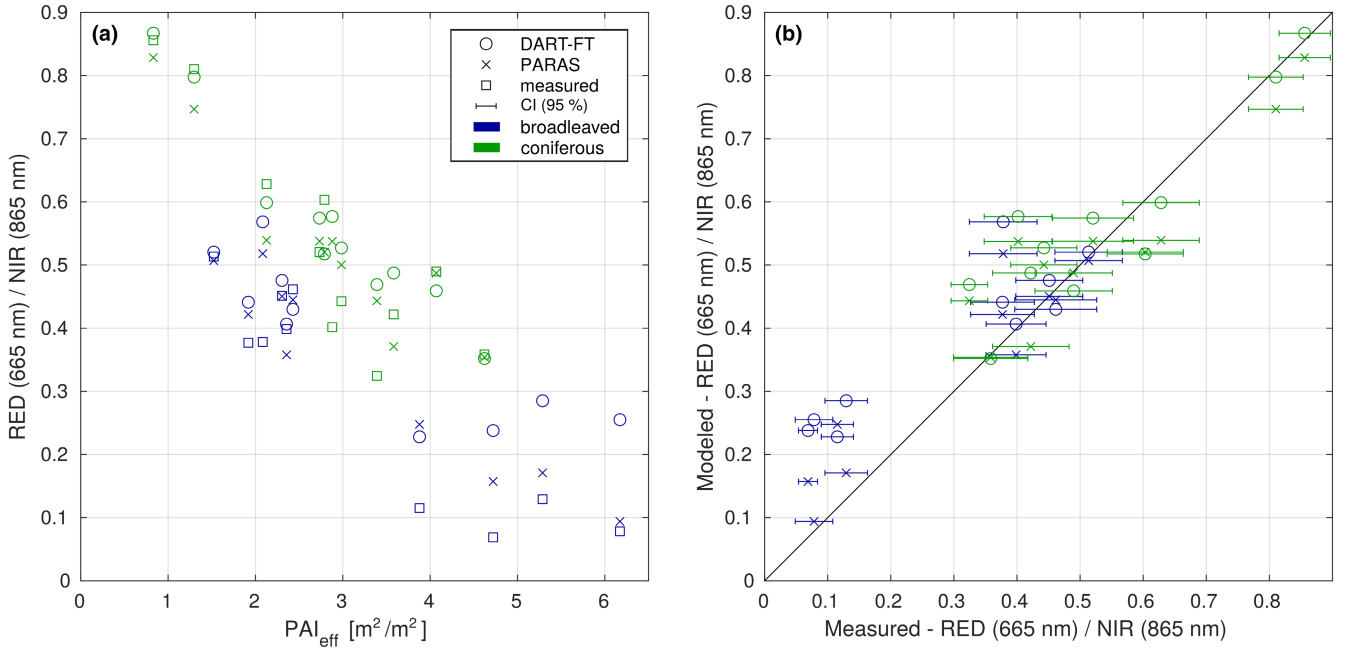

FIGURE 3 Red (665 nm) to near-infrared (NIR, 865 nm) canopy transmittance ratios measured and simulated with the DART-FT and PARAS models. Each point represents the mean red-to-NIR ratio in a forest plot, with broadleaved-dominated plots marked in blue and coniferous-dominated in green colour. The symbols indicate the simulated (with DART-FT or PARAS models) and measured values. The error bars mark the 95% confidence intervals (CI) of the in situ measurements, calculated as CI = mean ± 1.96 × (standard error of the mean). (a) Red-to-NIR transmittance ratio against effective plant area index (PAI_{eff}). (b) Simulated against measured red-to-NIR transmittance ratio.

3.2 | Sensitivity analyses

To explain the model performance differences between the visible and other wavelengths, we repeated the simulations by setting the reflectance and transmittance of all canopy elements and the reflectance of forest floor to zero. The contribution of scattering (by the canopy and forest floor) to the canopy transmittance was then quantified by comparing the results to those obtained with the default parameterization in Section 3.1. The average contribution of scattering to canopy transmittance was the smallest in the visible region (2%–13% in relative terms, 0.003–0.019 in absolute transmittance units), slightly larger in RE1 and SWIR2 bands (8%–29% relative, 0.013–0.048 absolute) and the largest in the NIR region (30%–62% relative, 0.087–0.204 absolute) (Table S3). Thus, the contribution of scattering to canopy transmittance is small in the visible region, and the errors in canopy gap fraction estimates are the main source of simulated to measured transmittance differences in this spectral region.

To further explain whether the slightly larger model overestimation of canopy transmittance in the red-edge and NIR, compared to the visible region, could be explained by inaccuracies in the input spectra, we conducted sensitivity analyses, where (i) the reflectance properties of woody elements were replaced by those of foliage, and (ii) the reflectance and transmittance of all canopy elements were decreased by 10%. The latter represents our estimate for maximum measurement and sampling uncertainties in the NIR canopy element spectra. A significant increase in canopy transmittance, and corresponding decrease in model performance in the NIR, was found to be associated with replacement of the woody elements by foliage (Table 2). On the other hand, the decrease of reflectance and transmittance of canopy elements by 10% improved the model agreement with in situ measurements (Table 2).

4 | DISCUSSION

Our first objective was to evaluate the performance of the two modelling approaches against in situ measurements. We observed very strong correlations between simulated and measured canopy spectral transmittance. The model errors for plot-level mean transmittance were small (RMSE up to 0.052) in the visible, RE1 and SWIR2 bands (Table 1), where scattering has a small contribution to the canopy transmittance (Table S3). This indicates that the canopy gap fraction data, that is, hemispherical photos used as input for both modelling approaches, were reasonably accurate. There were only a few plots, where somewhat larger errors in canopy gap fractions, and thus notable differences between simulated and measured transmittance, were observed (Figure 1). These errors could have been caused by inaccuracies in the image binarization, or by differences between the canopy gap fraction estimates (which represented an average over all azimuth directions) and the actual canopy gap fraction in the direction of the sun. Since past studies have focused mainly on the validation of models for canopy transmittance in the visible or photosynthetically active wavelength region (e.g. Majasalmi et al., 2014; Ni et al., 1997), the most novel findings in our study are related to the performance of the models at longer

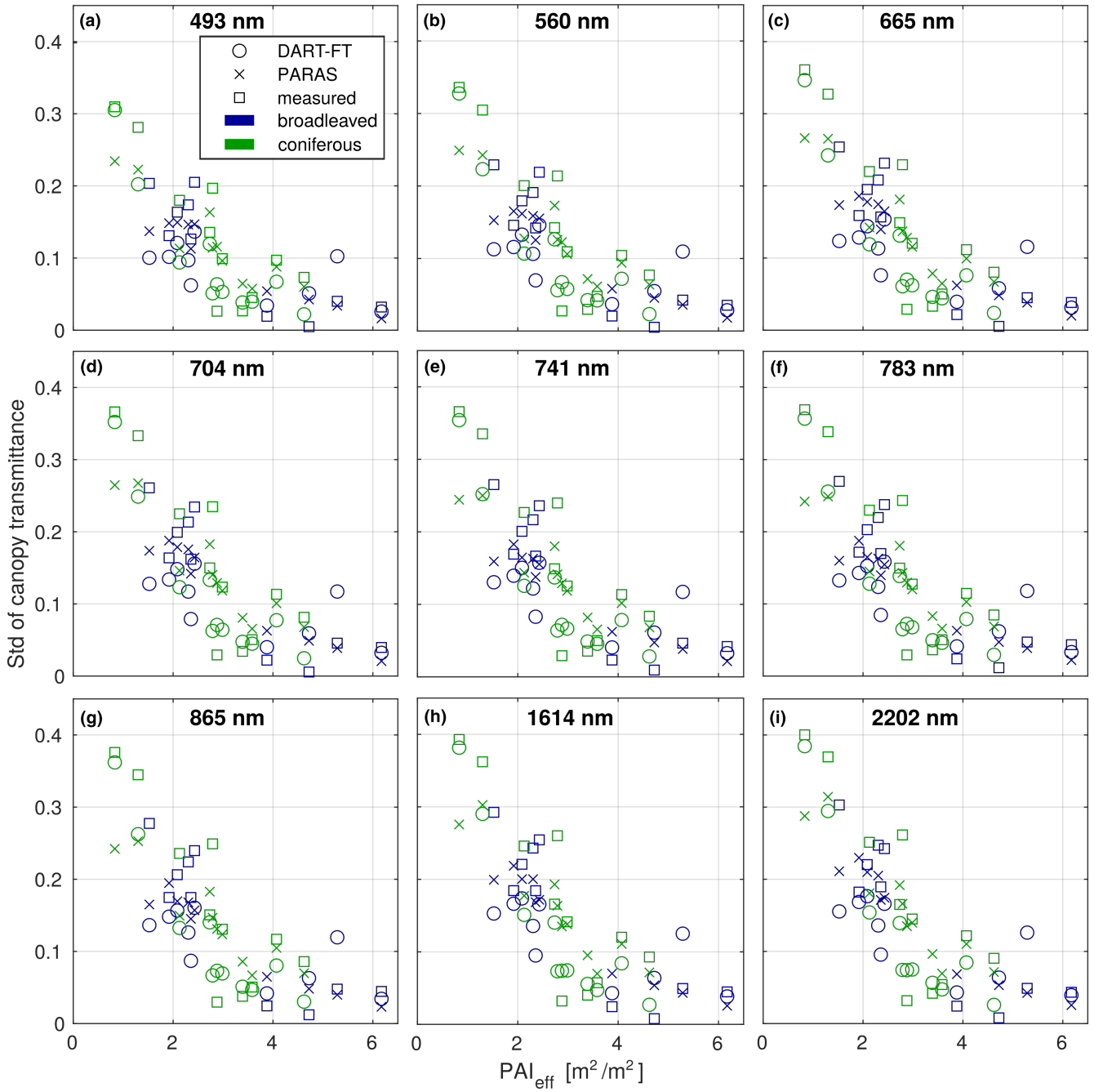

FIGURE 4 Dependence of standard deviation (std) of forest canopy spectral transmittance at nine spectral bands on the effective plant area index (PAI_{eff}). Each point represents the std of transmittance within a forest plot, with broadleaved-dominated plots marked in blue and coniferous-dominated in green colour. The symbols indicate the simulated (with DART-FT or PARAS models) and measured transmittance values.

wavelengths (i.e. NIR and SWIR bands), and reproducing the spectral dependence of the canopy transmittance. We observed that the model errors were the largest in the NIR and red-edge regions. However, the errors were not notably large and could be explained by uncertainties in the input spectra. Hence, the general spectral behaviour, such as the measured differences in the red-to-NIR transmittance ratio between tree species (Figure 3), was successfully reproduced by both models.

We also demonstrated that both models were able to reproduce the increase of within-stand spatial variability of canopy spectral transmittance with decreasing canopy density. Our results are in line with the findings of Kükenbrink et al. (2019), who compared DART model simulations to in situ measurements of the irradiance field under a single tree and demonstrated the capability of the DART model in reproducing the spatial and spectral variability in the radiation transmitted by the tree crown. The capability of the models to reproduce the spatial variability is a very promising finding, as the spatial variability of the below-canopy radiation regime has an influence on, for example, species richness (De Pauw et al., 2021; Helbach et al., 2022) and productivity (Rosati et al., 2020) of forest

TABLE 2 Statistics quantifying the differences between simulated and field-measured canopy spectral transmittance (DART-FT-measured, PARAS-measured), and between the two models (PARAS-DART-FT) in the near-infrared spectral band when the spectral input of the models were changed.

Scenario	r^2			Mean difference			RMSE			Relative RMSE (%)		
	DART-FT-measured	PARAS-measured	PARAS-DART-FT	DART-FT-measured	PARAS-measured	PARAS-DART-FT	DART-FT-measured	PARAS-measured	PARAS-DART-FT	DART-FT-measured	PARAS-measured	PARAS-DART-FT
Broadleaved												
Replace woody elements by foliage	0.84	0.90	0.95	0.078	0.134	0.056	0.100	0.147	0.069	37	54	20
Decrease element albedos by 10%	0.84	0.89	1.00	−0.001	−0.003	−0.013	0.057	0.048	0.021	21	18	9
Conifers												
Replace woody elements by foliage	0.94	0.94	0.99	0.081	0.094	0.013	0.093	0.104	0.029	45	51	10
Decrease element albedos by 10%	0.94	0.94	0.96	0.021	0.008	−0.002	0.050	0.046	0.031	24	22	11

floor vegetation. The spatial variability of canopy transmittance depends on the scale of the model simulations, that is, the voxel size in DART-FT and the segment size of the hemispherical photos in PARAS. The influence of these parameters on the simulations constitutes a future research topic.

The second objective was to compare the two modelling approaches to each other. From a practical viewpoint, it is beneficial that the computationally efficient and easy-to-parameterize PARAS is similar in performance compared to the turbid-medium crown approach of DART-FT. A good agreement between both models was observed in the conifer forest group. In broadleaved forests, where DART-FT slightly outperformed PARAS, the between-model differences were not notably large either. The PARAS model simulations have previously been compared against empirical data of forest reflectance factors (Hovi et al., 2022; Rautiainen & Stenberg, 2005), transmittance of photosynthetically active radiation (Majasalmi et al., 2014) and broadband albedo (Kuusinen et al., 2014). Our findings confirm *p*-theory as a promising tool capable of simulating spectral transmittance of forest canopies almost as accurately as more complex radiative transfer modelling with turbid-medium crowns.

Although our data covered a wide range of canopy structures from temperate to boreal forests, further studies should investigate the generalizability and transferability of our findings to forest types of other biomes and to more extreme illumination conditions (overcast sky and/or more extreme solar angles). The radiation regime of forest canopies is important for the productivity and biodiversity of the forest floor vegetation; yet it is undergoing changes due to climate-induced disturbances in forest canopy structure (de Frenne, 2023). From this perspective, the physically based simulation tools developed in this study can complement empirical radiation measurements (Hartikainen et al., 2020; Hertel et al., 2011; Hovi & Rautiainen, 2020) that are difficult to conduct for large areas or extensive periods of time. These tools can help us to study the interlinkages between radiation regime and forest floor productivity and biodiversity. Finally, the canopy transmittance contributes to remotely sensed signals, and thus its accurate simulation is essential for correct interpretations of optical remote sensing observations of forests.

AUTHOR CONTRIBUTIONS

Aarne Hovi: Conceptualization, data curation, formal analysis, investigation, methodology and writing—original draft. Růžena Janoutová: Conceptualization, data curation, formal analysis, investigation, methodology, visualization and writing—review and editing. Zbyněk Malenovský: Conceptualization and writing—review and editing. Daniel Schraik: Data curation, investigation and writing—review and editing. Jean-Philippe Gastellu-Etchegorry and Nicolas Lauret: Software and writing—review and editing. Jan Novotný: Conceptualization and writing—review and editing. Miina Rautiainen: Conceptualization, funding acquisition, project administration and writing—review and editing.

ACKNOWLEDGEMENTS

We thank Petri Forsström, Jussi Juola, Mait Lang, Jan Pisek, Lucie Homolová, Mihkel Kaha, Bijay Karki, Zuzana Lhotáková, Petr Lukeš, Titta Majasalmi and Ville Ranta for contributions in data collection. This study has received funding from the European Research Council (ERC) under the European Union's Horizon 2020 research and innovation programme (grant agreement no. 771049). The text reflects only the authors' view and the agency is not responsible for any use that may be made of the information it contains. The leaf spectral data from Lanžhot were collected under the project funded by the Ministry of Education, Youth and Sports of the Czech Republic, grant number LTAUSA18154.

CONFLICT OF INTEREST STATEMENT

The authors declare no conflict of interest.

DATA AVAILABILITY STATEMENT

The canopy transmittance, foliage and forest floor spectra, as well as forest inventory, hemispherical photograph and terrestrial laser scanning data are available via https://doi.org/10.23729/9a8d90cd-73e2-438d-9230-94e10e61adc9 (Hovi, Schraik, et al., 2024). We also utilized data from https://doi.org/10.3334/ORNLDAAC/336 (Spencer & Rock, 1999), http://www.aai.ee/bgf/ger2600/ (Lang et al., 2002) and https://doi.org/10.17632/pwfxgzz5fj.2 (Juola et al., 2022b) for stem bark spectra, and https://ads.atmosphere.copernicus.eu/cdsapp#!/dataset/cams-global-reanalysis-eac4 (CAMS, 2023) for atmosphere properties. The foliage angles were obtained from the scientific articles of Janoutová et al. (2019), Pisek et al. (2013, 2022), Raabe et al. (2015) and Stenberg et al. (1993). The DART model is available as an executable file after a licence agreement acceptance at https://dart.omp.eu/. The code used for conducting the PARAS model simulations and data analyses, as well as model input data derived from the above mentioned original datasets are available via https://doi.org/10.23729/5b4dc41c-eb63-4e57-9e92-191a96c54341 (Hovi, Janoutová, et al., 2024).

ORCID

Aarne Hovi https://orcid.org/0000-0002-4384-5279
Růžena Janoutová https://orcid.org/0000-0003-1830-7556
Zbyněk Malenovský https://orcid.org/0000-0002-1271-8103
Daniel Schraik https://orcid.org/0000-0002-7794-3918
Jean-Philippe Gastellu-Etchegorry https://orcid.org/0000-0002-6645-8837
Nicolas Lauret https://orcid.org/0000-0003-0594-6252
Jan Novotný https://orcid.org/0009-0004-1017-9160
Miina Rautiainen https://orcid.org/0000-0002-6568-3258

REFERENCES

Ballaré, C. L., & Austin, A. T. (2019). Recalculating growth and defense strategies under competition: Key roles of photoreceptors and jasmonates. *Journal of Experimental Botany*, *70*, 3425–3436. https://doi.org/10.1093/jxb/erz237

Brelsford, C. C., Nybakken, L., Kotilainen, T. K., Robson, T. M., & Polle, A. (2019). The influence of spectral composition on spring and autumn phenology in trees. *Tree Physiology*, *39*(6), 925–950. https://doi.org/10.1093/treephys/tpz026

CAMS. (2023). *CAMS global reanalysis (EAC4)*. Web page. https://ads.atmosphere.copernicus.eu/cdsapp#!/dataset/cams-global-reanalysis-eac4

Damm, A., Guanter, L., Verhoef, W., Schläpfer, D., Garbari, S., & Schaepman, M. E. (2015). Impact of varying irradiance on vegetation indices and chlorophyll fluorescence derived from spectroscopy data. *Remote Sensing of Environment*, *156*, 202–215. https://doi.org/10.1016/j.rse.2014.09.031

de Frenne, P. (2023). Novel light regimes in European forests. *Nature Ecology & Evolution*, *8*, 196–202. https://doi.org/10.1038/s41559-023-02242-2

De Pauw, K., Meeussen, C., Govaert, S., Sanczuk, P., Vanneste, T., Bernhardt-Römermann, M., Bollmann, K., Brunet, J., Calders, K., Cousins, S. A. O., Diekmann, M., Hedwall, P. O., Iacopetti, G., Lenoir, J., Lindmo, S., Orczewska, A., Ponette, Q., Plue, J., Selvi, F., … De Frenne, P. (2021). Taxonomic, phylogenetic and functional diversity of understorey plants respond differently to environmental conditions in European forest edges. *Journal of Ecology*, *109*, 2629–2648. https://doi.org/10.1111/1365-2745.13671

Ellis, C. R., Pomeroy, J. W., Essery, R. L. H., & Link, T. E. (2011). Effects of needleleaf forest cover on radiation and snowmelt dynamics in the Canadian Rocky Mountains. *Canadian Journal of Forest Research*, *41*, 608–620. https://doi.org/10.1139/X10-227

Emde, C., Buras-Schnell, R., Kylling, A., Mayer, B., Gasteiger, J., Hamann, U., Kylling, J., Richter, B., Pause, C., Dowling, T., & Bugliaro, L. (2016). The libRadtran software package for radiative transfer calculations (version 2.0.1). *Geoscientific Model Development*, *9*(5), 1647–1672. https://doi.org/10.5194/gmd-9-1647-2016

Gastellu-Etchegorry, J.-P., Yin, T., Lauret, N., Cajgfinger, T., Gregoire, T., Grau, E., Feret, J.-B., Lopes, M., Guilleux, J., Dedieu, G., Malenovský, Z., Cook, B. D., Morton, D., Rubio, J., Durrieu, S., Cazanave, G., Martin, E., & Ristorcelli, T. (2015). Discrete anisotropic radiative transfer (DART 5) for modeling airborne and satellite spectroradiometer and LIDAR acquisitions of natural and urban landscapes. *Remote Sensing*, *7*(2), 1667–1701. https://doi.org/10.3390/rs70201667

Gastellu-Etchegorry, J.-P., Yin, T., Lauret, N., Grau, E., Rubio, J., Cook, B. D., Morton, D. C., & Sun, G. (2016). Simulation of satellite, airborne and terrestrial LiDAR with DART (I): Waveform simulation with quasi-Monte Carlo ray tracing. *Remote Sensing of Environment*, *184*, 418–435. https://doi.org/10.1016/j.rse.2016.07.010

Hartikainen, S. M., Pieristè, M., Lassila, J., & Robson, T. M. (2020). Seasonal patterns in spectral irradiance and leaf UV-A absorbance under forest canopies. *Frontiers in Plant Science*, *10*, 1–16. https://doi.org/10.3389/fpls.2019.01762

Helbach, J., Frey, J., Messier, C., Mörsdorf, M., & Scherer-Lorenzen, M. (2022). Light heterogeneity affects understory plant species richness in temperate forests supporting the heterogeneity–diversity hypothesis. *Ecology and Evolution*, *12*(2), e8534. https://doi.org/10.1002/ece3.8534

Hertel, C., Leuchner, M., & Menzel, A. (2011). Vertical variability of spectral ratios in a mature mixed forest stand. *Agricultural and Forest Meteorology*, *151*, 1096–1105. https://doi.org/10.1016/j.agrformet.2011.03.013

Hovi, A., Janoutová, R., Malenovský, Z., Schraik, D., Gastellu-Etchegorry, J.-P., Lauret, N., Novotný, J., & Rautiainen, M. (2024). *Physically-based modeling of spectral transmittance through forest canopies: Data and code*. Aalto University. https://doi.org/10.23729/5b4dc41c-eb63-4e57-9e92-191a96c54341

Hovi, A., & Rautiainen, M. (2020). Spectral composition of shortwave radiation transmitted by forest canopies. *Trees*, *34*, 1499–1506. https://doi.org/10.1007/s00468-020-02005-7

Hovi, A., Schraik, D., Hanuš, J., Homolová, L., Juola, J., Lang, M., Lukeš, P., Pisek, J., & Rautiainen, M. (2022). Assessment of a photon recollision probability based forest reflectance model in European boreal and temperate forests. *Remote Sensing of Environment*, *269*, 112804. https://doi.org/10.1016/j.rse.2021.112804

Hovi, A., Schraik, D., Hanuš, J., Lukeš, P., Lhotáková, Z., Homolová, L., & Rautiainen, M. (2024). *A spectral-structural characterization of European temperate, hemiboreal and boreal forests: Laboratory and field data*. Aalto University. https://doi.org/10.23729/9a8d90cd-73e2-438d-9230-94e10e61adc9

Inness, A., Ades, M., Agustí-Panareda, A., Barr, J., Benedictow, A., Blechschmidt, A. M., Jose Dominguez, J., Engelen, R., Eskes, H., Flemming, J., Huijnen, V., Jones, L., Kipling, Z., Massart, S., Parrington, M., Peuch, V. H., Razinger, M., Remy, S., Schulz, M., & Suttie, M. (2019). The CAMS reanalysis of atmospheric composition. *Atmospheric Chemistry and Physics*, *19*(6), 3515–3556. https://doi.org/10.5194/acp-19-3515-2019

Janoutová, R., Homolová, L., Malenovský, Z., Hanuš, J., Lauret, N., & Gastellu-Etchegorry, J.-P. (2019). Influence of 3D spruce tree representation on accuracy of airborne and satellite forest reflectance simulated in DART. *Forests*, *10*, 292. https://doi.org/10.3390/f10030292

Juola, J., Hovi, A., & Rautiainen, M. (2022a). A spectral analysis of stem bark for boreal and temperate tree species. *Ecology and Evolution*, *12*(3), 1–14. https://doi.org/10.1002/ece3.8718

Juola, J., Hovi, A., & Rautiainen, M. (2022b). A dataset of stem bark reflectance spectra for boreal and temperate tree species. *Mendeley Data*, *V2*. https://doi.org/10.17632/pwfxgzz5fj.2

Kükenbrink, D., Hueni, A., Schneider, F. D., Damm, A., Gastellu-Etchegorry, J.-P., Schaepman, M. E., & Morsdorf, F. (2019). Mapping the irradiance field of a single tree: Quantifying vegetation-induced adjacency effects. *IEEE Transactions on Geoscience and Remote Sensing*, *57*(7), 4994–5011. https://doi.org/10.1109/TGRS.2019.2895211

Kükenbrink, D., Schneider, F. D., Schmid, B., Gastellu-Etchegorry, J.-P., Schaepman, M. E., & Morsdorf, F. (2021). Modelling of three-dimensional, diurnal light extinction in two contrasting forests. *Agricultural and Forest Meteorology*, *296*, 108230. https://doi.org/10.1016/j.agrformet.2020.108230

Kuusinen, N., Lukeš, P., Stenberg, P., Levula, J., Nikinmaa, E., & Berninger, F. (2014). Measured and modelled albedos in Finnish boreal forest stands of different species, structure and understory. *Ecological Modelling*, *284*, 10–18. https://doi.org/10.1016/j.ecolmodel.2014.04.007

Lang, A. R. G., & Xiang, Y. (1986). Estimation of leaf area index from transmission of direct sunlight in discontinuous canopies. *Agricultural and Forest Meteorology*, *37*(3), 229–243. https://doi.org/10.1016/0168-1923(86)90033-X

Lang, M., Kuusk, A., Nilson, T., Lükk, T., Pehk, M., & Alm, G. (2002). *Reflectance spectra of ground vegetation in sub-boreal forests*. Tartu Observatory. http://www.aai.ee/bgf/ger2600/

Majasalmi, T., Rautiainen, M., & Stenberg, P. (2014). Modeled and measured fPAR in a boreal forest: Validation and application of a new model. *Agricultural and Forest Meteorology*, *189–190*, 118–124. https://doi.org/10.1016/j.agrformet.2014.01.015

Malenovský, Z., Regaieg, O., Yin, T., Lauret, N., Guilleux, J., Chavanon, E., Duran, N., Janoutová, R., Delavois, A., Meynier, J., Medjdoub, G., Yang, P., van der Tol, C., Morton, D., Cook, B. D., & Gastellu-Etchegorry, J.-P. (2021). Discrete anisotropic radiative transfer modelling of solar-induced chlorophyll fluorescence: Structural impacts in geometrically explicit vegetation canopies. *Remote Sensing of Environment*, *263*, 112564. https://doi.org/10.1016/j.rse.2021.112564

Mayer, B., & Kylling, A. (2005). Technical note: The libRadtran software package for radiative transfer calculations—Description and examples of use. *Atmospheric Chemistry and Physics*, *5*(7), 1855–1877. https://doi.org/10.5194/acp-5-1855-2005

Mõttus, M., & Stenberg, P. (2008). A simple parameterization of canopy reflectance using photon recollision probability. *Remote Sensing of Environment*, *112*(4), 1545–1551. https://doi.org/10.1016/j.rse.2007.08.002

Musselman, K. N., Pomeroy, J. W., & Link, T. E. (2015). Variability in shortwave irradiance caused by forest gaps: Measurements, modelling, and implications for snow energetics. *Agricultural and Forest Meteorology*, *207*, 69–82. https://doi.org/10.1016/j.agrformet.2015.03.014

Ni, W., Li, X., Woodcock, C. E., Roujean, J.-L., & Davis, R. E. (1997). Transmission of solar radiation in boreal conifer forests: Measurements and models. *Journal of Geophysical Research: Atmospheres*, *102*(D24), 29555–29566. https://doi.org/10.1029/97JD00198

Ni-Meister, W., Yang, W., & Kiang, N. Y. (2010). A clumped-foliage canopy radiative transfer model for a global dynamic terrestrial ecosystem model. I: Theory. *Agricultural and Forest Meteorology*, *150*(7), 881–894. https://doi.org/10.1016/j.agrformet.2010.02.009

Nobis, M., & Hunziker, U. (2005). Automatic thresholding for hemispherical canopy-photographs based on edge detection. *Agricultural and Forest Meteorology*, *128*, 243–250. https://doi.org/10.1016/j.agrformet.2004.10.002

Pisek, J., Diaz-Pines, E., Matteucci, G., Noe, S., & Rebmann, C. (2022). On the leaf inclination angle distribution as a plant trait for the most abundant broadleaf tree species in Europe. *Agricultural and Forest Meteorology*, *323*, 109030. https://doi.org/10.1016/j.agrformet.2022.109030

Pisek, J., Sonnentag, O., Richardson, A. D., & Mõttus, M. (2013). Is the spherical leaf angle distribution a valid assumption for temperate and boreal broadleaf tree species? *Agricultural and Forest Meteorology*, *169*, 186–194. https://doi.org/10.1016/j.agrformet.2012.10.011

Raabe, K., Pisek, J., Sonnentag, O., & Annuk, K. (2015). Variations of leaf inclination angle distribution with height over the growing season and light exposure for eight broadleaf tree species. *Agricultural and Forest Meteorology*, *214–215*, 2–11. https://doi.org/10.1016/j.agrformet.2015.07.008

Rautiainen, M., Lukeš, P., Homolová, L., Hovi, A., Pisek, J., & Mõttus, M. (2018). Spectral properties of coniferous forests: A review of in situ and laboratory measurements. *Remote Sensing*, *10*(2), 1–28. https://doi.org/10.3390/rs10020207

Rautiainen, M., Mõttus, M., Yáñez-Rausell, L., Homolová, L., Malenovský, Z., & Schaepman, M. E. (2012). A note on upscaling coniferous needle spectra to shoot spectral albedo. *Remote Sensing of Environment*, *117*, 469–474. https://doi.org/10.1016/j.rse.2011.10.019

Rautiainen, M., & Stenberg, P. (2005). Application of photon recollision probability in coniferous canopy reflectance simulations. *Remote Sensing of Environment*, *96*(1), 98–107. https://doi.org/10.1016/j.rse.2005.02.009

Rosati, A., Wolz, K. J., Murphy, L., Ponti, L., & Jose, S. (2020). Modeling light below tree canopies overestimates net photosynthesis and radiation use efficiency in understory crops by averaging light in space and time. *Agricultural and Forest Meteorology*, *284*, 107892. https://doi.org/10.1016/j.agrformet.2019.107892

Savitzky, A., & Golay, M. J. E. (1964). Smoothing and differentiation of data by simplified least squares procedures. *Analytical Chemistry*, *36*, 1627–1639. https://doi.org/10.1021/ac60214a047

Schraik, D., Wang, D., Hovi, A., & Rautiainen, M. (2023). Quantifying stand-level clumping of boreal, hemiboreal and temperate European forest stands using terrestrial laser scanning. *Agricultural and Forest Meteorology*, *339*, 109564. https://doi.org/10.1016/j.agrformet.2023.109564

Smith, H. (1982). Light quality, photoperception, and plant strategy. *Annual Review of Plant Physiology*, *33*, 481–518. https://doi.org/10.1146/annurev.pp.33.060182.002405

Spencer, S., & Rock, B. N. (1999). *BOREAS TE-08 Aspen bark spectral reflectance data*. Data set. Oak Ridge National Laboratory Distributed Active Archive Center. https://doi.org/10.3334/ORNLDAAC/336

Stenberg, P. (2007). Simple analytical formula for calculating average photon recollision probability in vegetation canopies. *Remote Sensing of Environment*, *109*(2), 221–224. https://doi.org/10.1016/j.rse.2006.12.014

Stenberg, P., Lukeš, P., Rautiainen, M., & Manninen, T. (2013). A new approach for simulating forest albedo based on spectral invariants. *Remote Sensing of Environment*, *137*, 12–16. https://doi.org/10.1016/j.rse.2013.05.030

Stenberg, P., Smolander, H., & Kellomäki, S. (1993). Description of crown structure for light interception models: Angular and spatial distribution of shoots in young scots pine. In S. Linder & S. Kellomäki (Eds.), *Management of structure and productivity of boreal and subalpine forests* (pp. 43–50). Studia Forestalia Suecica 191.

Widlowski, J., Mio, C., Disney, M., Adams, J., Andredakis, I., Atzberger, C., Brennan, J., Busetto, L., Chelle, M., Ceccherini, G., Colombo, R., Côté, J., Eenmäe, A., Essery, R., Gastellu-etchegorry, J., Gobron, N., Grau, E., Haverd, V., Homolová, L., … Zenone, T. (2015). The fourth phase of the radiative transfer model intercomparison (RAMI) exercise: Actual canopy scenarios and conformity testing. *Remote Sensing of Environment*, *169*, 418–437. https://doi.org/10.1016/j.rse.2015.08.016

Widlowski, J. L., Pinty, B., Clerici, M., Dai, Y., de Kauwe, M., de Ridder, K., Kallel, A., Kobayashi, H., Lavergne, T., Ni-Meister, W., Olchev, A., Quaife, T., Wang, S., Yang, W., Yang, Y., & Yuan, H. (2011). RAMI4PILPS: An intercomparison of formulations for the partitioning of solar radiation in land surface models. *Journal of Geophysical Research: Biogeosciences*, *116*, G02019. https://doi.org/10.1029/2010JG001511

Widlowski, J.-L., Pinty, B., Lopatka, M., Atzberger, C., Buzica, D., Chelle, M., Disney, M., Gastellu-Etchegorry, J.-P., Gerboles, M., Gobron, N., Grau, E., Huang, H., Kallel, A., Kobayashi, H., Lewis, P. E., Qin, W., Schlerf, M., Stuckens, J., & Xie, D. (2013). The fourth radiation transfer model intercomparison (RAMI-IV): Proficiency testing of canopy reflectance models with ISO-13528. *Journal of Geophysical Research: Atmospheres*, *118*(13), 6869–6890. https://doi.org/10.1002/jgrd.50497

SUPPORTING INFORMATION

Additional supporting information can be found online in the Supporting Information section at the end of this article.

Table S1: Summary of forest canopy structure variables and tree species proportions in the study plots.

Table S2: Tree species present in the study plots, and leaf angle distributions used for them in the DART-FT model.

Table S3: Mean change in canopy spectral transmittance simulated with DART-FT and PARAS models when the reflectance and transmittance of the canopy elements and forest floor were set to zero.

Figure S1: Layout of the measurement grids in a plot.

Figure S2: Overview of the 3D forest scenes used for canopy transmittance simulations in DART.

Figure S3: Illustration of tree parameterization in the DART model using an ellipsoid composed of two half-ellipsoids, which represent the upper and lower parts of the crown.

Figure S4: Dependence of forest canopy spectral transmittance at nine spectral bands on the effective plant area index (PAI_{eff}).

How to cite this article: Hovi, A., Janoutová, R., Malenovský, Z., Schraik, D., Gastellu-Etchegorry, J.-P., Lauret, N., Novotný, J., & Rautiainen, M. (2024). Physically based modelling of spectral transmittance through forest canopies. *Methods in Ecology and Evolution*, *15*, 1859–1872. https://doi.org/10.1111/2041-210X.14402